







FULL PAPER

Temperature dependence on phase evolution in the BaTiO₃ polytypes studied using ab initio calculations

Marisa C. Oliveira¹  | Renan A. P. Ribeiro²  | Elson Longo²  |
 Maurício R. D. Bomio¹  | Fabiana V. Motta¹  | Sergio R. de Lazaro³ 

¹LSQM – Laboratory of Chemical Synthesis of Materials, Department of Materials Engineering, Federal University of Rio Grande do Norte, Natal, Brazil

²CDMF-UFSCar, Federal University of São Carlos, São Carlos, Brazil

³Department of Chemistry, State University of Ponta Grossa, Ponta Grossa, Brazil

Correspondence

Renan A. P. Ribeiro, CDMF-UFSCar, Federal University of São Carlos, PO Box 676, São Carlos, SP 13565-905, Brazil.
 Email: ribeiroapr@gmail.com

Funding information

Conselho Nacional de Desenvolvimento Científico e Tecnológico, Grant/Award Number: 156176/2018-1; Coordenação de Aperfeiçoamento de Pessoal de Nível Superior, Grant/Award Number: 2019/88887.319041; Federal University of Rio Grande do Norte; Federal University of São Carlos; Fundação Araucária; Fundação de Amparo à Pesquisa do Estado de São Paulo, Grant/Award Number: 2013/07296-2; State University of Ponta Grossa

Abstract

Identifying the forces that drive a temperature-induced phase transition is always challenging in the prospect of the first-principles methods. Herein, we perform a first-principles study of the temperature effects on structural, energetic, electronic, and vibrational properties of four BaTiO₃ polymorphs using quasi-harmonic approximations. Study of the stability between these four phases, which we break into contributions arising from the vibration of the lattice, electronic structure, and volume expansion/contraction, is helpful to confirm the sequence of phase transitions as cubic → tetragonal → orthorhombic → rhombohedral, as well as its transition temperatures. A general mechanism was proposed based on the combination between structural distortions at [TiO₆] clusters, vibrational characteristics, and electronic structure. These findings confirm the power of quasi-harmonic approximations to disclose the main fingerprints associated with both thermic and mechanical phase transitions, serving as a guide for further theoretical studies.

KEYWORDS

BaTiO₃, DFT, phase transition, temperature-dependent, BTO

1 | INTRODUCTION

BaTiO₃ (BTO) is a typical perovskite oxide with a band gap energy of nearly 3.2 eV^[1] with an ABO₃ perovskite cubic structure^[2,3] and has been studied using several theoretical and experimental methods. Its study under high pressure has been reported by many authors in the last few decades using different methods such as dielectric measurements, Brillouin scattering, Raman scattering, X-ray diffraction, and the photoacoustic technique.^[4–8] In a recent study,^[9] experimental results for pressure-strained BaTiO₃ show that it first undergoes a phase transition from the tetragonal to orthorhombic/rhombohedral phase occurring above ~2.6 GPa, and then it finally goes to the cubic phase above 8.4 GPa, the phase transition being from tetragonal to cubic at room temperature reported around 2 GPa.

One of the most important features of BTO is related to the electrical properties such as ferroelectric, piezoelectric, and pyroelectric features.^[10] This compound has a paraelectric to ferroelectric phase transition below the Curie point near 120°C.^[11] The influence of temperature for phase transition is very accentuated, with several polymorphs being possible for BTO material; the crystal structure changes among from rhombohedral (*R3m*) to orthorhombic (*Amm2*) at 183 K, then to tetragonal (*P4mm*) at 278 K and to cubic (*Pm3̄m*) at 403 K. The cubic phase is paraelectric and the other phases are ferroelectric, exhibiting a nonzero dipole moment that depends on the temperature. There is one BTO formula unit in the unit cell in all four phases, so that phase transitions to ferroelectric phases are due to the soft mode at the C point of the cubic BTO Brillouin zone (BZ).^[12–17]

The phase transitions in BTO single crystals are very interesting due to the structural distortions, which enable the connection between the polymorphs, as well as the understanding of structure-properties relationships, increasing the scientific interest about the mechanism related to the phase transitions.^[18–20] Experimental observations have demonstrated that the sequence of decreasing temperature phase transitions is more complex and as follows: cubic-tetragonal-orthorhombic-rhombohedral. For these ferroelectric phases, the spontaneous polar directions are also accordingly changing from the $\langle 100 \rangle$ axis to the $\langle 110 \rangle$ axis, and then to the $\langle 111 \rangle$ axis as the temperature decreases.^[21–24]

A deeper understanding of phase transition mechanisms is one of the most fundamental phenomena of matter, being an interesting topic with increased attention being paid by theoreticians. However, from the theoretical point of view, identification of the main forces that drive a phase transition induced by temperature is challenging, as pressure-induced phase transitions are routinely investigated by employing density functional theory (DFT)-based methods. Although first-principles methods are extremely precise, they are commonly restricted to studying the electronic structure at 0 K, requiring innovative approaches such as atomistic simulations.^[25–28] In this context, the quasi-harmonic approximation (QHA) arises as an interesting and alternative tool capable of computing the quasi-harmonic thermal properties of solids beyond the harmonic approximation. In this context, the explicit volume dependence of phonon frequencies can be calculated with QHA by retaining the simple harmonic expression for the Helmholtz free energy of the system (F). This method also allows for combining pressure and temperature effects on the structural, elastic, and thermodynamic properties of materials.^[29]

Aiming to gain deeper insights into the temperature-driven phase transition of BTO, the purpose of the present work fulfills three objectives: (a) to develop a first-principles-based computational approach capable of modeling the BTO in a wide compositional and temperature range; (b) to present and discuss the theoretical results in comparison to the experimental measurement, indicating the temperature-induced phase evolution of bulk BTO from the paraelectric to ferroelectric phase; and (c) to elucidate the relationship between structural and electronic features with the phase evolution for this material.

2 | COMPUTATIONAL DETAILS

In this work, first-principles total-energy calculations were carried out within the periodic DFT framework using the CRYSTAL17 software package.^[29] The hybrid PBE0 exchange-correlation functional was implemented in all calculations^[30]; Ti, O, and Ba centers were described by 8-6411 (d311f), 6-31d1G, and 9766331311G all-electron basis sets, respectively, available at the CRYSTAL^[31] and MykeTowler^[32] basis-set webpage.

Diagonalization of the Fock matrix was performed at adequate k -point grids in the reciprocal space, which depends on the phase under treatment using Pack-Monkhorst/Gilat^[33] shrinking factors ($IS = ISP = 4$). The calculations were carried out with truncation criteria for the Coulomb and exchange series controlled by a set of five thresholds (10^{-8} , 10^{-8} , 10^{-8} , 10^{-8} , and 10^{-14}). It is important to point out that the CRYSTAL17 code requires the description of primitive unit cell vectors and Wyckoff positions to enable constructing symmetry-adapted wavefunctions used in the DFT formalism. The initial atomic positions and lattice parameters were set according to a previous theoretical study developed by Evarestov and Bandura.^[12] In addition, the Raman vibrational modes and their corresponding wavenumbers were calculated using numerical second derivatives of the total energy.

The most recent version of the CRYSTAL code implemented an automated scheme for computing the QHA crystal properties, which relies on computing and fitting harmonic vibration frequencies at different volumes after having performed volume-constrained geometry optimizations. In all QHA calculations, a volume range extending from a – 3% compression to a + 6% expansion concerning the equilibrium unit cell volume was considered. In this interval, four equidistant volumes were used for volume-constrained geometry optimization and frequencies calculations. In this context, one of the powerful advantages of the QHA is allowing a natural combination of pressure and temperature effects on the structural and elastic properties of materials, therefore being a good tool to investigate temperature-induced phase transitions.^[29,34–36]

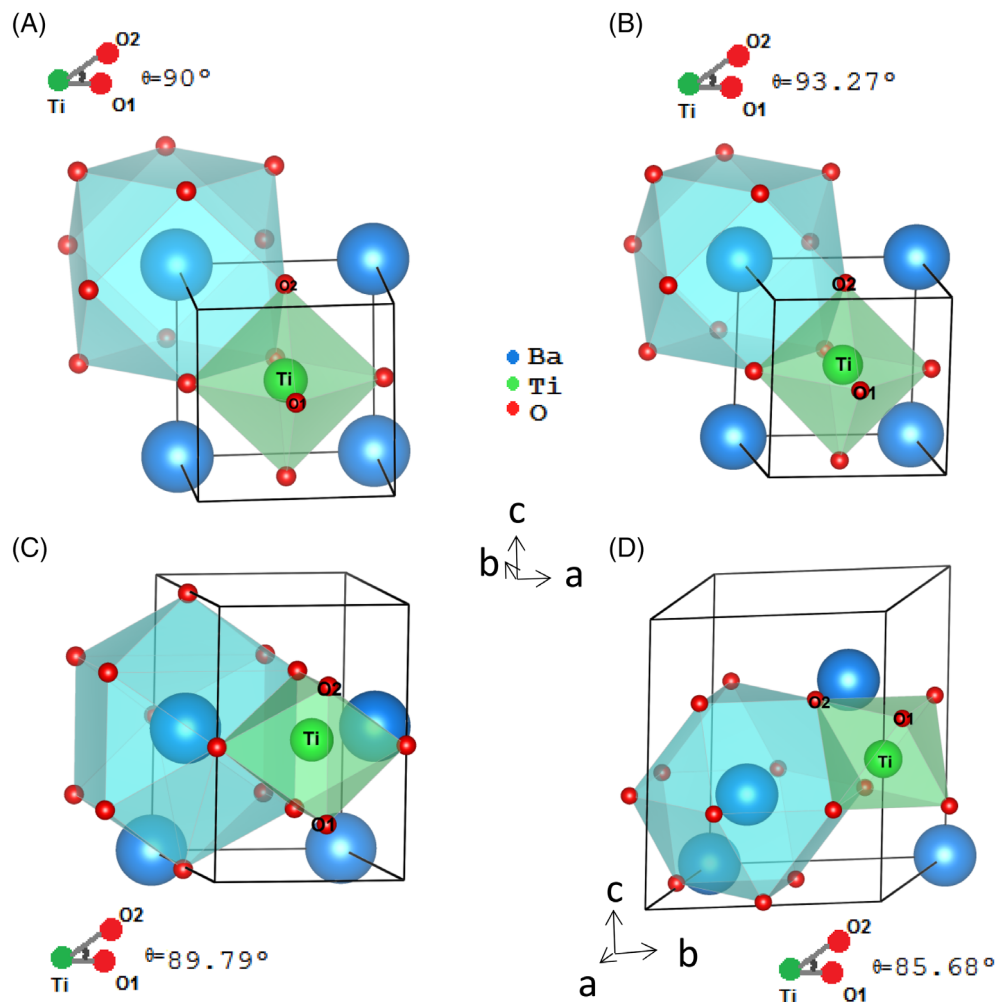
3 | RESULTS AND DISCUSSION

3.1 | Crystal structure and electronic properties

Understanding the main differences between the crystalline structures of the polymorphs involved in the phase transition corresponds to an important step on the disclosure of the mechanism involved in such process. Indeed, the connection between different polymorphs is strictly associated with the creation, breaking, or distortion effects regarding the chemical bonds. Thus, four phases were considered for BTO in this study, and the optimized crystal structure for each polymorph is represented in Figure 1A–D.

Figure 1A–D illustrates a schematic representation of BTO clusters constituent of cubic, tetragonal, orthorhombic, and rhombohedral structure perovskites, with space group symmetries of $Pm\bar{3}m$, $P4mm$, $Amm2$, and $R3m$, respectively. The Ti atoms are coordinated to six O atoms in all cases, producing octahedral $[TiO_6]$ clusters (with 6 vertices, 8 faces, and 12 edges). Correspondingly, the Ba atoms are coordinated to twelve O atoms, resulting in $[BaO_{12}]$ clusters (with 12 vertices, 12 faces, and 30 edges). The main difference between BTO cubic and tetragonal phase is a slight displacement in octahedral $[TiO_6]$ clusters with the theta angle from 90° to $\sim 93.3^\circ$ (Figure 1A,B), while orthorhombic and rhombohedral

FIGURE 1 Schematic representation of BTO clusters constituent (A) cubic, (B) tetragonal, (C) orthorhombic, and (D) rhombohedral polymorphs



phase results in a theta angle from $\sim 89.8^\circ$ to $\sim 85.7^\circ$. Also, such representations are found to be in excellent agreement with the results obtained by Evarestov and Bandura, following the Wyckoff positions of atoms with the site symmetry group.^[12]

The after mentioned off-center displacement for Ti atoms is commonly found in perovskite materials, being responsible for the superior dielectric and ferroelectric properties associated with the second-order Jahn-Teller effect arising from the bonding overlap between Ti(3d) and O(2p) orbitals. From a theoretical point of view, the structural distortions can result in a redistribution of the electronic density among the crystalline structure, especially for the $[\text{TiO}_6]$ clusters where the distortion can be assigned to the order-disorder originated from the off-centering cation displacement, which modifies the local chemical environment on the ferroelectric perovskites.^[37]

Concerning the relation between structural and electronic properties for BTO polymorphs, the electronic structure was investigated to ascertain information about the chemical environment and its electronic state distribution. First, the Band Structure profiles calculated within the primitive BZ path for the different BTO polymorphs are displayed in Figure 2A-D. In this case, the Band Structures of the BaTiO_3 polymorphs were calculated using 10 k -points (cubic), 18 k -points (tetragonal), 21 k -points (orthorhombic), and 13 k -points (rhombohedral) along the appropriate high-symmetry paths of the proper BZ.

The analysis of the Band Structures and Density of States (DOS) indicated the bandgap value for the four BTO polymorphs. The band gap is closely related to the difference in the energy level between the Valence Band (VB) and the Conduction Band (CB), which can be originated from structural distortions in the material. Furthermore, structural distortions and bandgap play an important role in the electronic properties, such as photocatalytic activity and photoluminescence, as well as serve as a guide to interpret the ferroelectric properties of the materials.^[37]

The Band Structures of the four BTO polymorphs indicate that the cubic $Pm\bar{3}m$ structure presents a direct bandgap energy of 4.68 eV at Γ (0,0,0), the tetragonal $P4mm$ structure presents an indirect bandgap energy of 4.73 eV from $A(1/2,1/2,1/2)$ to Γ , and the orthorhombic $Amm2$ structure presents an indirect bandgap energy of 5.06 eV from $T(1/2,1/2,1/2)$ to Γ , whereas the rhombohedral $R3m$ structure has an indirect bandgap of 5.18 eV from $L(0,1/2,1/2)$ to Γ . In this case, the bandgap order can be described as cubic < tetragonal < orthorhombic < rhombohedral.

A general analysis of the DOS projected on atoms and orbitals is presented in Figure 3A-D.

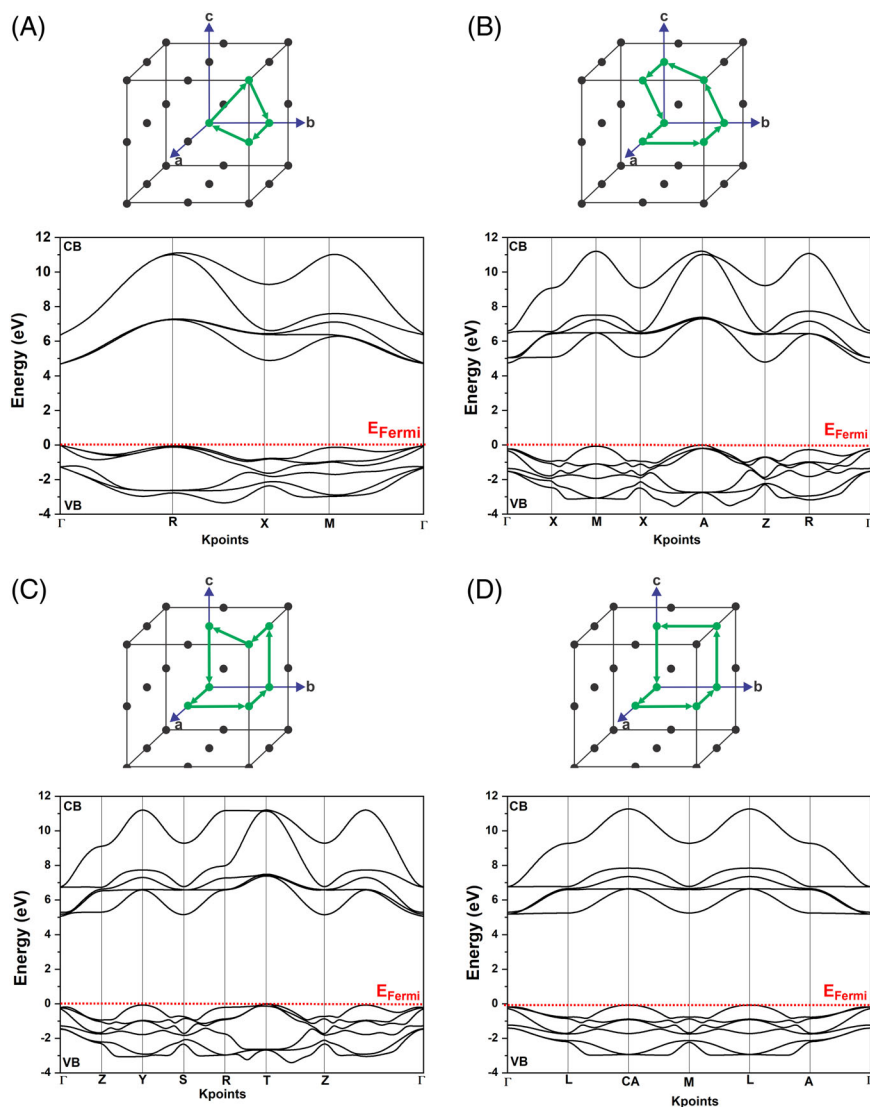


FIGURE 2 Calculated primitive Brillouin zone and band structure for the BaTiO₃ polymorphs (A) cubic, (B) tetragonal, (C) orthorhombic, and (D) rhombohedral

DOS shows that the upper part of the VB mainly consists of O 2p (p_x , p_y , p_z) orbitals with a minor extent of Ba and Ti orbitals. On the other hand, the lower part of the CB is mostly derived from Ti 3d (d_{xz} , d_{xy} , d_{yz} , d_{z^2} , $d_{x^2-y^2}$) orbitals in all polymorphs.

The bandgap energy (E_{gap}) values calculated with the PBE0 functional in this work, as well as the available theoretical and experimental data, are shown in Table 1. The calculated values show a reasonable agreement with the previous theoretical and experimental results, especially with regard to the bandgap order. Also, the obtained results indicate that the exchange-correlation function has a great influence on calculating the band gap values.

Let us now briefly analyze the electronic structure of the ferroelectric polymorphs depicted in both Figures 2B-D and 3B-D. In all cases, the Valence Band Maximum is mainly composed of O 2p (p_x , p_y , p_z) states, whereas the Conduction Band Minimum (CBM) shows singular composition following the tetragonal, orthorhombic, and rhombohedral structures. Indeed, the CBM for the tetragonal phase (Figure 3B) is composed of Ti ($3d_{yz}$) states, while the orthorhombic phase shows a CBM formed by Ti ($3d_{xy}$) (Figure 3C), and the rhombohedral phase (Figure 3D) has a mixed composition of Ti states at CBM with a major extent of $3d_{z^2}$ than $3d_{xy}$. This fact suggests that $[\text{TiO}_6]$ clusters for the different phases show a singular distortion axis, in agreement with the expected spontaneous polar directions for these polymorphs. Moreover, the calculated bandgap values for the ferroelectric polymorphs indicate that CBM shifts with regard to the energy range, suggesting that such a frontier crystalline orbital is sensitive to the bonding overlap between Ti-O atoms, in agreement with the ferroelectric order in such polymorphs.

3.2 | The phase transitions—Temperature phase diagram

Aiming to construct a temperature phase diagram and analyses of the relative stability of the different BTO phases, the QHA approach was implemented to compute the Helmholtz free energy (F) and its dependence on temperature. The relative Helmholtz free energy difference (ΔF) was computed to build the temperature phase diagram using a reference state in the proper transition, as presented in Figure 4. To help the

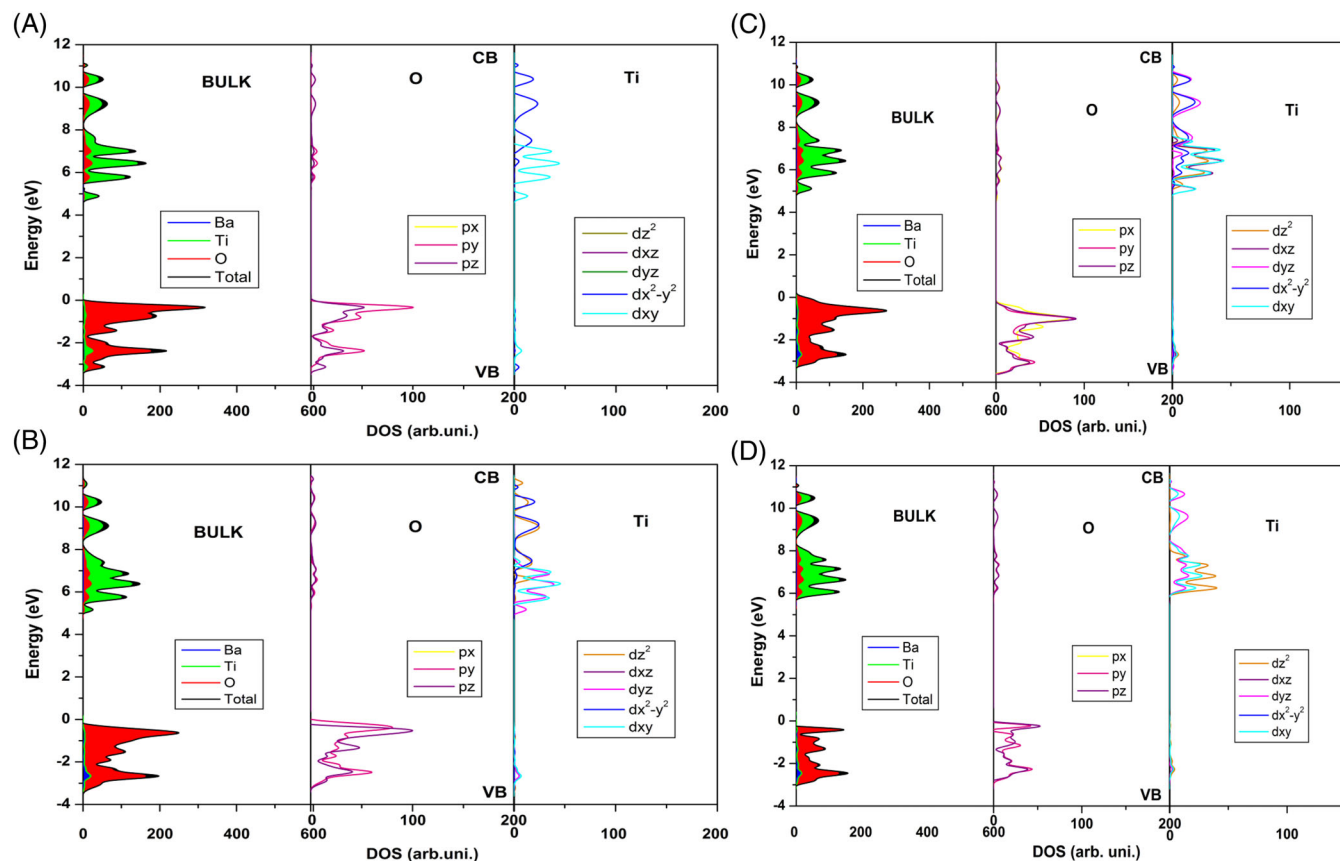


FIGURE 3 Calculated bulk and projected on atoms and orbitals DOS for the BaTiO_3 polymorphs (A) cubic, (B) tetragonal, (C) orthorhombic, and (D) rhombohedral

TABLE 1 Theoretical and experimental values of the band gap for BaTiO_3 polymorphs

	This work	Theor. ^a	Theor. ^b	Theor. ^c	Exp. ^d	Exp. ^e	Exp. ^f
Cubic	4.68 eV	3.70 eV	4.00 eV	1.77 eV	3.20 eV	3.23 eV	3.70 eV
Tetragonal	4.73 eV	3.15 eV	4.10 eV	1.81 eV	3.40 eV	3.12 eV	3.90 eV
Orthorhombic	5.06 eV	—	4.70 eV	2.38 eV	—	—	—
Rhombohedral	5.18 eV	—	4.90 eV	2.46 eV	—	—	—

^aRef. [4].

^bRef. [12].

^cRef. [38].

^dRef. [39].

^eRef. [40].

^fRef. [16].

understand the referred phase transitions, additional phase diagrams are depicted in Figure S1 containing individual plots of Helmholtz free energy difference in each investigated phase transition. The temperature-induced phase transition calculations show that BaTiO_3 undergoes three phase transitions: from cubic $Pm\bar{3}m$ to tetragonal $P4mm$ between 300 and 320 K, then to orthorhombic $Amm2$ around 250 K to 280 K, and finally to rhombohedral $R3m$ at 200 K to 240 K. Here, it is important to point out that each phase transition is investigated considering that other phases were not formed in the range. Figure 4 shows the sequence of phase transitions as follows: cubic \rightarrow tetragonal \rightarrow orthorhombic \rightarrow rhombohedral. Indeed, despite the deviations in the calculation of transition temperature in comparison to the experimental results,^[10,41] the obtained results show good agreement regarding the description of the relative stability of BTO polymorphs with respect to the temperature.

Theoretically, we can calculate the structural parameters accompanying the phase transition and demonstrate how the cubic phase is transformed into the tetragonal, orthorhombic, and rhombohedral phases. For this, we considered the temperature range from 0 K to 500 K at a pressure of 0 GPa for the evaluation of lattice parameters and unit cell volume. The overall effect of temperature on the volume and unit cell parameters for the four polymorphs is presented in Table 2. We also considered the thermomechanical effect through different pressures of ~ 1 GPa and ~ 1.5 GPa concerning different polymorphs, as presented in Table S1.

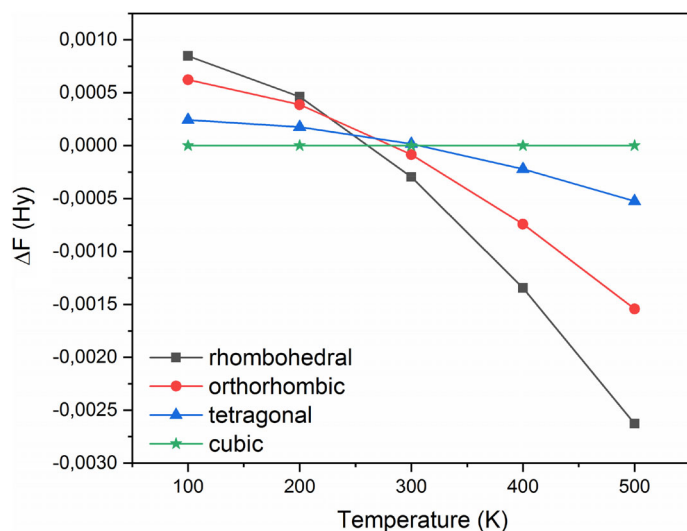


FIGURE 4 Calculated temperature phase diagrams for BaTiO₃ with the PBE0 functional, considering the existence of cubic, tetragonal, orthorhombic, and rhombohedral phases

The volumes and lattice parameters of cubic and tetragonal BaTiO₃ polymorphs increase uniformly against temperature at a pressure of 0 GPa, whereas the volumes and lattice parameters of the orthorhombic and rhombohedral polymorphs decrease with increasing temperature at a pressure of 0 GPa using the PBE0 functional. The increase of the lattice parameters with the increase in the temperature was calculated as 0.82% for the cubic and 0.36% tetragonal phases, whereas a decrease of the lattice parameters for the orthorhombic and rhombohedral phases is approximately 1.35% and 2.7%. Similar results were found considering the inclusion of mechanical strain (pressure) (Table S1), that is, an increase in volume and lattice parameters for cubic and tetragonal structures and a reduction of volume and lattice parameters for orthorhombic and rhombohedral structures. In this case, it is possible to confirm that the cubic to the tetragonal phase transition is a first-order phase transition followed by volume expansion, whereas the further transitions are accompanied by a volume contraction.

The ferroelectric phase transition can conceptually be interpreted as a phase evolution driven by a structural distortion. From the chemical perspective, this interpretation is only possible due to the fundamental concept of solid mechanics deformation, which is intrinsically associated with the chemical nature resulting from attractive and repulsive forces.^[42] Therefore, the phase evolution regarding the polymorphs of BTO proportionally modifies the equilibrium between attractive and repulsive forces of solids through the chemical bond of [BaO₁₂] and [TiO₆] clusters in them. In this context, a careful analysis of the electron density distribution is helpful to understand and correlate the main changes associated with the phase transition. Thus, electron density maps were computed with the aim of deeply characterizing the temperature-driven ferroelectric transitions, as presented in Figure 5.

In this analysis, the electronic density isolines around cations and oxygen atoms can show the formation of chemical bonds through an accumulation of charge (isolines) in the bond path, as well as the formation of electronic dipoles through a charge separation between consecutive bonds. A careful analysis of electron density distribution for the rhombohedral phase (Figure 5A) clearly indicates the formation of electronic dipoles due to the charge separation between Ti-O-Ti intermetallic connection, that is, electron density is more centered along one of the Ti-O bond paths along the [111] direction, confirming that the spontaneous polar direction is the eight <111> axis. Similar results were noted for the orthorhombic phase (Figure 5B), with the polar direction being the twelve <110> axis. On the other hand, the polar directions for the tetragonal phase (Figure 5C) are the six <100> axis with increased charge separation between Ti-O-Ti intermetallic connection. For the cubic paraelectric phase (Figure 5D), the calculated electron density map confirms the isometric distribution of the electron density along with all Ti-O chemical bonds resulting from a null dipole moment along with the crystalline structure.

Therefore, it is possible to point out that the cubic to the tetragonal phase transition is followed by an off-centering displacement of Ti cations induced by a tetragonal distortion under heating. The following transitions can be addressed for a structural rearrangement of the Ti atom along the [TiO₆] clusters, resulting in different distortion degrees. These facts can be pointed out from Figure 5, where the charge separation clarifies the charge concentration along the ferroelectric dipole following the order of tetragonal > orthorhombic > rhombohedral. Indeed, a large charge separation was obtained for tetragonal BTO in comparison to the other phases, that is, a large extent of the total electron density is mainly centered along one of Ti-O bond in the Ti-O-Ti bond path, in agreement with the experimental findings for the ferroelectric order.^[10,41]

3.3 | Temperature-dependent and vibrational properties

Based on the crystallography, the group theory analysis and symmetry indicate that titanate crystals with a tetragonal perovskite-type structure of the *P4mm* space group with the site symmetry *C*_{4v}¹ show Raman-active modes described as 4E Transverse (TO) + Longitudinal (LO) optical

TABLE 2 Calculated lattice parameters and unit cell volume with the PBE0 functional as a function of the temperature of the four studied BaTiO₃ polymorphs

BaTiO ₃ (cubic)—Pressure 0 GPa				
Temperature (K)	Cell volume (Å) ³	Lattice parameters $a = b = c$ (Å)		
0	60.697	3.9299		
100	60.898	3.9343		
200	60.928	3.9349		
300	60.971	3.9359		
400	61.022	3.9370		
500	61.075	3.9381		
BaTiO ₃ (tetragonal)—Pressure 0 GPa				
Temperature (K)	Cell volume (Å) ³	Lattice parameters (Å)		
		$a = b$	c	
0	61.155	3.9214	3.9769	
100	61.200	3.9221	3.9785	
200	61.216	3.9223	3.9791	
300	61.230	3.9225	3.9796	
400	61.243	3.9227	3.9800	
500	61.256	3.9229	3.9805	
BaTiO ₃ (orthorhombic)—Pressure 0 GPa				
Temperature (K)	Cell volume (Å) ³	Lattice parameters (Å)		
		a	b	c
0	61.326	3.9184	5.5883	5.6012
100	61.220	3.9196	5.5832	5.5949
200	61.190	3.9192	5.5822	5.5937
300	61.144	3.9187	5.5806	5.5919
400	61.092	3.9180	5.5789	5.5899
500	61.037	3.9174	5.5769	5.5877
BaTiO ₃ (rhombohedral)—Pressure 0 GPa				
Temperature (K)	Cell volume (Å) ³	Lattice parameters (Å)		
		$a = b$	c	
0	61.340	5.5729	6.8417	
100	61.184	5.5685	6.8353	
200	61.097	5.5660	6.8317	
300	60.979	5.5626	6.8268	
400	60.843	5.5587	6.8212	
500	60.692	5.5543	6.8150	

phonons + 3A₁(TO + LO) + B₁(TO + LO), while all modes for the cubic phase ($Pm\bar{3}m$) are Raman inactive, and therefore no first-order Raman can be observed.^[43,44]

According to the theoretical results obtained with the PBE0 functional for the tetragonal phase, the obtained frequency (ω) range is from ~200 cm⁻¹ to ~600 cm⁻¹, as presented in Table 3, as well as its dependence on the temperature. In this case, one imaginary frequency was found for the tetragonal phase, indicating a structural instability from soft modes as reported in previous theoretical studies^[12] as a consequence of frequency calculations carried out at low temperature.

First, the obtained results reported herein are in agreement with previous studies.^[11,16] The information obtained in Table 3 is useful for analyzing different atom displacements in vibrational modes at different temperatures. For example, in the tetragonal phase, a slight reduction in ω is mainly noted at higher frequencies (500 cm⁻¹-600 cm⁻¹) of 0.466 cm⁻¹ and 1.097 cm⁻¹, respectively. Furthermore, these peaks located at 592.203 cm⁻¹ and 559.074 cm⁻¹ may be assigned to bending vibration of [TiO₆] and [BaO₁₂] clusters, evidencing the temperature-driven

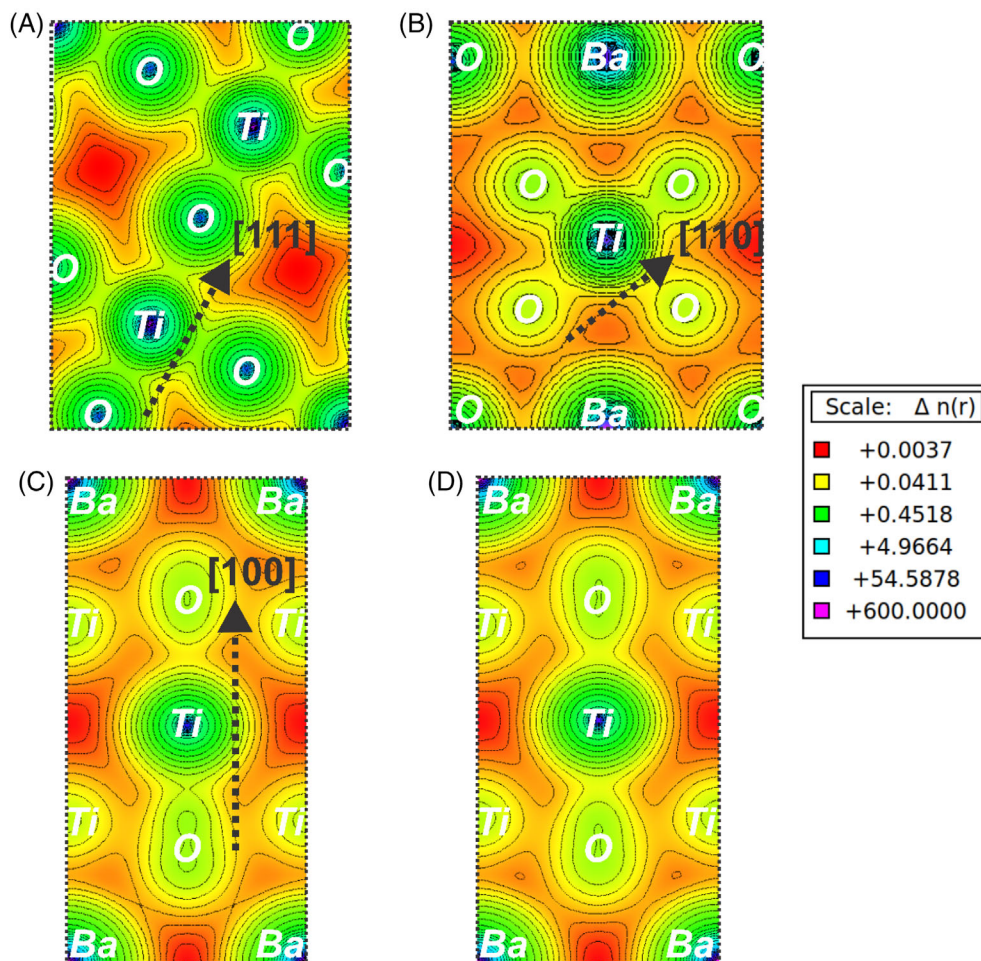


FIGURE 5 Electron density maps for A, rhombohedral, B, orthorhombic, C, tetragonal and D, cubic phases of BaTiO₃

BaTiO ₃ (P4mm, C _{4v} ¹)					
Raman mode	Temperature (K)				
	100	200	300	400	500
	ω (cm ⁻¹)				
E	129.401i	129.938i	130.639i	131.309i	132.096i
A ₁	200.756	200.171	200.018	199.665	200.214
E	206.385	206.267	206.195	206.107	205.987
A ₁	329.480	329.063	328.656	328.485	327.802
B ₁	359.656	359.576	359.508	359.452	359.308
E	359.834	359.817	359.799	359.774	359.751
E	559.074	558.937	558.828	558.727	558.608
A ₁	592.203	591.845	591.582	591.339	591.106

TABLE 3 Calculated Raman modes at the PBE0 level of theory for tetragonal BaTiO₃ and its dependence on the temperature

structural distortions. Furthermore, according to the literature,^[45–47] the Raman mode experimental around 300 cm⁻¹ is characteristic of the tetragonal BaTiO₃, being an important mode to assign the structural phase transition. Usually, this mode is assigned as a triple degenerated mode originating from the overlap between LO-TO and B₁ modes. Therefore, the dynamical evaluation of this mode can indicate the stability of the tetragonal phase, once in the vicinity of T_c, this mode disappears and the cubic phase becomes stable.^[45–47] Theoretically, in this frequency range (300–360 cm⁻¹), a reduction of vibration was observed at 1.678 cm⁻¹ for A₁, 0.348 cm⁻¹ for B₁, and 0.083 for E modes, confirming that external temperature can act on the structural deformation softening the characteristic vibrational mode of tetragonal BaTiO₃ up to the phase transition.

The obtained Raman modes for the orthorhombic $Amm2$ and rhombohedral $R3m$ phases of $BaTiO_3$ structure are shown in Table S2, with the orthorhombic phase being described by $\Gamma = 4A_1 + A_2 + 3B_1 + 4B_2$ Raman-active modes, while rhombohedral polymorph exhibits $\Gamma = 3A_1 + 4E$ active modes, in agreement with the previous results.^[8,12] Combining the structural analysis with the calculated Raman modes dependence on temperature for the orthorhombic and rhombohedral phase, it is possible to observe that a decrease in volume and lattice parameters generated an increase in ω of vibration with the increase in the temperature. The inverse was observed for the tetragonal case, increasing the temperature, increasing the volume and lattice parameters, followed by a decrease in ω of vibration. This fact may be associated with the resulting local structural distortions produced through the metals more strongly interacting with anions in orthorhombic and rhombohedral phases, and thereby distorts the octahedron to give the resultant upward shift of the Raman mode in question.

4 | CONCLUSIONS

We calculated the structural, vibrational, and the electronic properties of four polytypes of $BaTiO_3$, $Pm\bar{3}m$ $P4mm$, $Amm2$, and $R3m$ structures using ab initio calculations with DFT and PBE0 functionals using the CRYSTAL17 code. Lattice parameters, energy gaps, temperature dependency, and Raman frequencies were calculated for the four polytypes. The phase transitions were calculated using ab initio quasi-harmonic calculations and by an analysis of a temperature diagram. The bandgaps of the four polytypes in the $BaTiO_3$ structure were compared to previous predictions, confirming the ferroelectric order and electronic features associated with the structural distortion of such phases. Phase transitions in $BaTiO_3$ and some aspects of the local atomic-scale structure were revealed combining QHA calculations with Raman spectroscopy, where the general mechanism associated with the temperature-driven phase transition for $BaTiO_3$ is presented, showing good agreement with the experimental results. In this context, we can argue that such a protocol can serve as a guide for further investigations regarding both thermic and mechanical induced phase transitions for solid-state materials.

ACKNOWLEDGEMENTS

This work was supported by the Federal University of São Carlos, State University of Ponta Grossa, Federal University of Rio Grande do Norte (PPGCeM-UFRN), CAPES, CNPq, FAPESP (2013/07296-2), and the Fundação Araucária. R.A.P. Ribeiro acknowledges financial support from CNPq (156176/2018-1). M.C. Oliveira acknowledges the financial support from PNPd/CAPES (2019/88887.319041).

ORCID

Marisa C. Oliveira  <https://orcid.org/0000-0003-3392-7489>

Renan A. P. Ribeiro  <https://orcid.org/0000-0002-4128-8296>

Elson Longo  <https://orcid.org/0000-0001-8062-7791>

Maurício R. D. Bomio  <https://orcid.org/0000-0001-9016-4217>

Fabiana V. Motta  <https://orcid.org/0000-0002-3523-737X>

Sergio R. de Lázaro  <https://orcid.org/0000-0001-9753-7936>

REFERENCES

- [1] T. Chen, J. Meng, S. Wu, J. Pei, Q. Lin, X. Wei, J. Li, Z. Zhang, *J. Alloys Compd.* **2018**, 754, 184.
- [2] C. Fu, N. Chen, G. Du, *Ceram. Int.* **2017**, 43, 15927.
- [3] S. Utara, S. Hunpratub, *Ultrason. Sonochem.* **2018**, 41, 441.
- [4] V. Mishra, A. Sagdeo, V. Kumar, M. K. Warshi, H. M. Rai, S. K. Saxena, D. R. Roy, V. Mishra, R. Kumar, P. R. Sagdeo, *J. Appl. Phys.* **2017**, 122, 065105.
- [5] A. Boochani, G. Rasoolian, F. Kafi, A. Aminian, S. M. Elahi, *Chin. J. Phys.* **2019**, 59, 357.
- [6] J. Gao, H. Zhang, L. Xie, J. Yu, G. Wang, Y. Gu, H. He, J. Bai, *J. Eur. Ceram. Soc.* **2017**, 37, 985.
- [7] R. Y. Sato-Berrú, E. V. Mejía-Uriarte, C. Frausto-Reyes, M. Villagrán-Muniz, H. M. S. J. M. Saniger, *Spectrochim. Acta A* **2007**, 66, 557.
- [8] Y.-S. Seo, J. S. Ahn, *Phys. Rev. B* **2013**, 88, 014114.
- [9] S. Tyagi, V. G. Sathe, G. Sharma, V. Srihari, H. K. Poswal, *J. Mater. Sci.* **2018**, 53, 7224.
- [10] M. Acosta, N. Novak, V. Rojas, S. Patel, R. Vaish, J. Koruza, G. A. Rossetti, J. Rödel, *Appl. Phys. Rev.* **2017**, 4, 041305.
- [11] X. Deng, H. Zhang, T. Li, D. Li, J. Li, X. Wang, L. Li, *Chin. Sci. Bull.* **2010**, 55, 2182.
- [12] R. A. Evarestov, A. V. Bandura, *J. Comput. Chem.* **2012**, 33, 1123.
- [13] P. Goudochnikov, A. J. Bell, *J. Phys. Condens. Matter* **2007**, 19, 176201.
- [14] H. T. Stokes, E. H. Kisi, D. M. Hatch, C. J. Howard, *Acta Crystallogr. B* **2002**, 58, 934.
- [15] J. J. Wang, P. P. Wu, X. Q. Ma, L. Q. Chen, *J. Appl. Phys.* **2010**, 108, 114105.
- [16] S. Sanna, C. Thierfelder, S. Wippermann, T. P. Sinha, W. G. Schmidt, *Phys. Rev. B* **2011**, 83, 054112.
- [17] P. Phaktapha, J. Jutimoosik, A. Bootchanont, P. Kidkhunthod, S. Rujirawat, R. Yimnirun, *Integr. Ferroelectr.* **2017**, 177, 74.

- [18] H. F. Kay, P. Vousden, *Philos. Mag.* **1949**, *40*, 1019.
- [19] S.-E. Park, S. Wada, L. E. Cross, T. R. Shrout, *J. Appl. Phys.* **1999**, *86*, 2746.
- [20] H. F. Kay, *Acta Crystallogr.* **1948**, *1*, 229.
- [21] O. L. G. Alderman, C. J. Benmore, J. Neuefeind, A. Tamaloni, R. Weber, *J. Phys. Condens. Matter* **2019**, *31*, 20LT01.
- [22] S. Mantri, J. E. Daniels, *IEEE Trans. Ultrason. Ferroelectr. Freq. Control* **2018**, *65*, 1517.
- [23] B. Ravel, E. A. Stern, R. I. Vedrinskii, V. Kraizman, *Ferroelectrics* **1998**, *206*, 407.
- [24] H. Zhang, *AIP Adv.* **2013**, *3*, 042118.
- [25] R. Lizárraga, F. Pan, L. Bergqvist, E. Holmström, Z. Gercsi, L. Vitos, *Sci. Rep.* **2017**, *7*, 3778.
- [26] B. Singh, M. K. Gupta, R. Mittal, S. L. Chaplot, *Phys. Chem. Chem. Phys.* **2018**, *20*, 12248.
- [27] S. Tinte, M. G. Stachiotti, M. Sepiarsky, R. L. Migoni, C. O. Rodriguez, *J. Phys. Condens. Matter* **1999**, *11*, 9679.
- [28] Y. Qi, S. Liu, I. Grinberg, A. M. Rappe, *Phys. Rev. B* **2016**, *94*, 134308.
- [29] R. Dovesi, A. Erba, R. Orlando, C. M. Zicovich-Wilson, B. Civalieri, L. Maschio, M. Rérat, S. Casassa, J. Baima, S. Salustro, B. Kirtman, *WIREs: Comput. Mol. Sci.* **2018**, *8*, e1360.
- [30] C. Adamo, V. Barone, *J. Chem. Phys.* **1999**, *110*, 6158.
- [31] CRYSTAL- Basis Sets Library, http://www.crystal.unito.it/Basis_Sets/Ptable.html (accessed: February 2019).
- [32] Mike Towler's CRYSTAL Resources Page, <http://www.tcm.phy.cam.ac.uk/~mdt26/crystal.html> (accessed: February 2019).
- [33] H. J. Monkhorst, J. D. Pack, *Phys. Rev. B* **1976**, *13*, 5188.
- [34] A. Erba, J. Maul, R. Demichelis, R. Dovesi, *Phys. Chem. Chem. Phys.* **2015**, *17*, 11670.
- [35] A. Erba, *J. Chem. Phys.* **2014**, *141*, 124115.
- [36] J. Maul, I. M. G. Santos, J. R. Sambrano, A. Erba, *Theor. Chem. Acc.* **2016**, *135*, 36.
- [37] R. A. P. Ribeiro, S. R. de Lazaro, *J. Alloys Compd.* **2017**, *714*, 553.
- [38] Q.-J. Liu, N.-C. Zhang, F.-S. Liu, H.-Y. Wang, Z.-T. Liu, *Opt. Mater.* **2013**, *35*, 2629.
- [39] S. H. Wemple, *Phys. Rev. B* **1970**, *2*, 2679.
- [40] S. Kappadan, T. W. Gebreab, S. Thomas, N. Kalarikkal, *Mater. Sci. Semicond. Process.* **2016**, *51*, 42.
- [41] B. Jiang, J. Iocozzia, L. Zhao, H. Zhang, Y.-W. Harn, Y. Chen, Z. Lin, *Chem. Soc. Rev.* **2019**, *48*, 1194.
- [42] R. A. P. Ribeiro, S. R. D. Lázaro, *Quím. Nova* **2014**, *37*, 1165.
- [43] C. J. Bradley, A. P. Cracknell, *The Mathematical Theory of Symmetry in Solids*, Clarendon, Oxford **1972**.
- [44] Bilbao Crystallographic Server: Structure IR Raman and Hyper-Raman Activity, <http://www.cryst.ehu.es/rep/sam.html> (accessed: February 2019).
- [45] Z. Lazarević, N. Romčević, M. Vijatović, N. Paunović, M. Romčević, B. Stojanović, Z. Dohčević-Mitrović, *Acta Phys. Pol. A* **2009**, *115*, 808.
- [46] H. Hayashi, T. Nakamura, T. Ebina, *J. Phys. Chem. Solid* **2013**, *74*, 957.
- [47] C. H. Perry, D. B. Hall, *Phys. Rev. Lett.* **1965**, *15*, 700.

SUPPORTING INFORMATION

Additional supporting information may be found online in the Supporting Information section at the end of this article.

How to cite this article: Oliveira MC, Ribeiro RAP, Longo E, Bomio MRD, Motta FV, de Lazaro SR. Temperature dependence on phase evolution in the BaTiO₃ polytypes studied using ab initio calculations. *Int J Quantum Chem.* 2020;120:e26054. <https://doi.org/10.1002/qua.26054>